AIAA JOURNAL
Vol. 31, No. 6, June 1993

Electric-Discharge Excited Blast Waves in a Flat Subsonic Nozzle

Paolo Luchini*
University of Naples, Naples 80125, Italy

The persistence of pressure waves generated by an electric discharge in the throat of a subsonic nozzle is studied analytically and numerically with particular reference to the operation of the high-power EUREKA excimer laser under construction at the national Italian ENEA Frascati laboratories. The attention is focused on transverse waves traveling parallel to the discharge electrodes. After some analytical estimates, a quasi-two-dimensional numerical simulation is presented of the propagation of these waves in the anticipated geometry of the discharge chamber of the EUREKA laser. The possibility of reflection of pressure waves on the thermal slug left behind by the previous discharge is also considered.

I. Introduction

In a high-power, high-repetition-rate excimer laser, gas flows at a subsonic speed through a nozzle of elongated cross section in the throat of which an electric discharge is periodically fired with a repetition rate of the order of 1 kHz. Only about 1% of the energy released by the discharge is usefully converted into electromagnetic waves in the laser cavity positioned at the throat of the nozzle. All of the remaining energy instantaneously heats up the gas, with respect to the propagation time of sound, and produces blast waves that, if still present in the discharge chamber when the next pulse fires, may cause instability of the following discharges. A one-dimensional picture of the phenomenon is shown in Fig. 1. The initial instantaneous temperature and pressure increase subsequently divides up into three waves: an entropy wave (the thermal slug), which travels with the main flow velocity V; and forward and backward pressure waves with velocity $V + a$ and $V - a$, respectively (a being the speed of sound).

In the simplified one-dimensional situation depicted in Fig. 1, these waves propagate out and do not interfere with following discharges if only enough time is allowed for all three waves to abandon the discharge volume. Provided that $V < a/2$, the slowest wave is the entropy wave; therefore, this criterion may be expressed figuratively by saying that the gas where one discharge has occurred must be washed out of the discharge volume before another discharge may be fired. However, various circumstances may disrupt such an ideal behavior:

1) If the pressure waves are strong enough to behave as shock waves, the entropy change through the backward wave may change the thermodynamical state of the gas arriving at the discharge section.

2) Obstacles or bends in the feed and exhaust ducts may reflect the waves back onto the discharge section.

3) Transverse waves, propagating at an angle with respect to the flow direction, may be excited by disuniformities in the discharge and come back on reflection by the lateral walls.

Problem 1 is not a major concern for the typical energy release during a discharge of the order of $50 \div 100$ J/l under a gas pressure of the order of some atmospheres. The shock strength can be calculated from the equation of state of an ideal gas to be given by

$$\delta p/p = (\gamma - 1)\, \delta e/p \qquad (1)$$

where $\delta p/p$ is the relative pressure change caused by the addition of an energy δe at constant volume, γ the ratio of specific heats, and δe and p must be expressed in the same units (for instance, J/m^3, which is the same as N/m^2). For an energy release of 100 J/l into a monoatomic gas ($\gamma = 5/3$) at 4 atm, Eq. (1) gives $\delta p/p = 0.16$. The dimensionless entropy increase through the shock wave is of the order of $(\delta p/p)^3/20$, i.e., 2×10^{-4}, and the same order of magnitude may be expected to be the change of the gas' thermodynamical properties behind the expansion wave that closes the wave train. Even more important, this change is uniform and, therefore, not harmful to following discharges. (In addition, the leading shock wave may in practice be weaker, or even totally absent, if the edge of the discharge is smooth rather than sharp.)

The importance of problem 2 is difficult to assess in general, as it depends on the particular geometrical configuration. It is, nevertheless, advisable to avoid creating undesired mirrors, for instance, by placing plane walls orthogonal to the line of sight from the discharge section or by introducing abrupt changes in cross section at a short distance from the discharge cell.

Problem 3 is the most troublesome because the lateral walls of the duct are necessarily orthogonal to the line of sight and do produce reflections. In this paper, we will concentrate on this problem. It must be emphasized that, in order to produce transverse waves, the discharge must be transversely disuniform in the first place because otherwise these waves would not be excited at all. Unavoidable strong disuniformities are, however, produced whenever the discharge does not fill up all of the volume available and terminates at a distance from the walls, as is necessary in order to avoid damage of the laser's mirrors.

In the elongated geometry typical of the discharge chamber of lasers, transverse waves propagating across the electrodes have characteristic frequencies much higher (of the order of 8 kHz for asymmetric and 16 kHz for symmetric modes for a chamber height of 3 cm) than those propagating along the electrodes (250 Hz for asymmetric and 500 Hz for symmetric modes for a chamber width of 1 m). It would therefore seem that the latter should be of greater concern because they interfere with laser operation at a lower frequency. On the other hand, cross-electrode waves couple more effectively to the thin electric discharge.

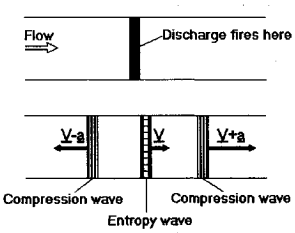

Fig. 1 Waves generated by an instantaneous release of energy in a gas flowing through a one-dimensional duct.

Received July 23, 1991; revision received April 26, 1992; accepted for publication April 26, 1992.

*Associate Professor, Istituto di Gasdinamica, Facoltà di Ingegneria, P.le Tecchio 80.

Published research papers are mostly concerned with quasi-one-dimensional numerical simulations of longitudinal waves going around the recirculation loop[1] and two-dimensional simulations[2] and experimental investigations[3] of transverse waves propagating across the electrodes.

Instead, we have investigated the pattern of waves propagating along the electrodes. This was also done by Baranov et al.,[4] however, the discharge geometry did not correspond to their experiment. Our numerical simulations refer to the actual configuration of the excimer laser under construction at the ENEA Frascati laboratories under the EUREKA sponsorship.

II. Analytical Estimates for a Uniform-Cross-Section Infinite Duct

Acoustic Approximation

The waves produced by the instantaneous energy release of the electric discharge (comparable to an explosion) are in principle shock waves, and their evolution should be calculated according to the full nonlinear Euler equations of fluid dynamics. Nevertheless, if their amplitude is not too strong, it may be sufficient to describe these waves by the linear acoustic wave equation.

The appropriate dimensionless parameter measuring the adequacy of the acoustic approximation is the ratio of the pressure variation δp accompanying the wave to the absolute pressure p. For instance, a typical nonlinear effect, the irreversible entropy increase caused by the passage of a shock wave, is of the order of $(\delta p/p)^3/20$. (There also are some nonlinear phenomena that may manifest themselves even when $\delta p/p$ is small, but they are associated with the long-term accumulation of nonlinear phase delays, leading, for instance, to the eventual breaking of a wave far from its source[5] and are not relevant in the present context.)

Since the maximum overpressure induced by the discharges we wish to consider is of the order of $0.1 \div 0.2$ in relative magnitude, and becomes half of that as soon as the two pressure waves have become spatially separated, we decided to adopt the acoustic-wave theory for our analytical and two-dimensional numerical calculations. The results of a one-dimensional nonlinear numerical calculation, reported in the Appendix, support this choice.

Linear pressure waves in a moving fluid are governed by the equation

$$\left[\left(\frac{1}{a}\frac{\partial}{\partial t}+M\frac{\partial}{\partial z}\right)^2-\Delta_2\right]\delta p=g \tag{2}$$

where δp is the pressure perturbation, z the coordinate in the direction of motion of the undisturbed fluid, which has a velocity V giving rise to the local Mach number $M = V/a$; and g a δ-function generation term, nonzero only where and when the discharge fires, the precise form of which may be dispensed for the present purposes because its effect can be represented by specifying the pressure jump occurring at the instant of the discharge.

Uniform, Constant-Cross-Section Duct

In an infinite uniform-cross-section duct, the solution of Eq. (2) may be obtained classically by separation of variables in the form of the modal expansion expressed by

$$\delta p=\sum_{m,n=0}^{\infty}F_{m,n}(z,\,t)\varphi_{m,n}(x,\,y) \tag{3}$$

where $\varphi_{m,n}$ turn out to be the eigenfunctions of the two-dimensional Helmholtz equation

$$\frac{\partial^2\varphi_{m,n}}{\partial x^2}+\frac{\partial^2\varphi_{m,n}}{\partial y^2}+\frac{\omega_{c,m,n}^2}{a^2}\varphi_{m,n}=0 \tag{4}$$

while $F_{m,n}$ obey the differential equation

$$\frac{1}{a^2}\frac{\partial^2F_{m,n}}{\partial t^2}+\frac{2M}{a}\frac{\partial^2F_{m,n}}{\partial t\partial z}-(1-M^2)\frac{\partial^2F_{m,n}}{\partial z^2}+\frac{\omega_{c,m,n}^2}{a^2}F_{m,n}=0 \tag{5}$$

In the particular case of a duct of rectangular cross section with sides A and B, $\varphi_{m,n}=\cos(m\pi x/A)\cos(n\pi y/B)$ and $\omega_{c,m,n}^2/a^2=(m\pi/A)^2+(n\pi/B)^2$. The mode with $m=n=0$ corresponds to purely longitudinal waves, of the kind that appears in Fig. 1; modes with $m\neq 0$ and $n=0$, if A is the longer dimension, represent transverse waves propagating parallel to the longer side (that is, in a laser, parallel to the electrodes), and modes with $m=1$ and higher represent waves having a component of motion along the shorter side (across the electrodes).

As far as Eq. (5) is concerned, modes differ from each other only for their cutoff frequency $\omega_{c,m,n}$. For the longitudinal mode ($m=n=0$) $\omega_{c,m,n}=0$, and, thus, Eq. (5) reduces to a one-dimensional wave equation, whose general homogeneous solution is well known to be of the form

$$F_{0,0}=f^+[z-(1+M)at]+f^-[z+(1-M)at] \tag{6}$$

In an electric-discharge excited laser, the generation term g of Eq. (1) is only nonzero for the duration of the discharge, i.e., a negligibly small time compared to the interval between pulses. After each shot, the pressure undergoes a finite increment, which can be calculated easily from Eq. (1), while the derivative $Dp/Dt=\partial p/\partial t+V\partial p/\partial z$ remains unchanged. From these two initial conditions, the two functions f^+ and f^- can be calculated easily, and the result is two nondispersive waves with the same shape as the discharge region propagating forward and backward in the guise of Fig. 1.

For nonlongitudinal modes, the situation is quite different: since the term $(\omega_{c,m,n}^2/a^2)F_{m,n}$ in Eq. (5) introduces dispersion, the two outgoing waves do not maintain their original shape, and the possibility exists that their tail might persist in the discharge region even at times so large that the longitudinal wave has moved out completely. This possibility can be studied analytically, as the Green function of Eq. (5) is known.

A few calculations that we do not report here (similar to those that may be found, for instance, in Ref. 6), give

$$F_{m,n}=\frac{1}{2a}\frac{\mathrm{D}}{\mathrm{D}t}J_0\{\omega_{c,m,n}[t^2-(z/a-Mt)^2]^{1/2}\} \tag{7}$$

as the solution of Eq. (5) that satisfies the conditions $F_{m,n}=\delta(z)$ and $DF_{m,n}/Dt=0$ at $t=0$.

We are particularly interested in the tail that the outgoing blast waves leave at the position of the discharge; that is, at the origin $z=0$. For $z=0$ Eq. (7) specializes to

$$\begin{aligned}F_{m,n}&=\frac{\omega_{c,m,n}}{2(1-M^2)^{1/2}a}J_0'[(1-M^2)^{1/2}\omega_{c,m,n}t]\\&=\frac{\omega_{c,m,n}}{2(1-M^2)^{1/2}a}\{\delta[(1-M^2)^{1/2}\omega_{c,m,n}t]\\&\quad-J_1[(1-M^2)^{1/2}\omega_{c,m,n}t]\}\end{aligned} \tag{8}$$

The tail is therefore expressed by the J_1 Bessel function, which has its maximum value of 0.58 for $s=(1-M^2)^{1/2}\omega_{c,m,n}t\simeq 1.8$ and the asymptotic expression $J_1(s)\simeq(2/\pi s)^{1/2}\cos(s-3\pi/4)$ for $s\gg 1$.

The just found asymptotic expression of the Green function for transverse modes in a uniform duct allows us to state that after a few oscillation periods ($\omega_{c,m,n}t\gg 1$) each mode leaves back at the origin a slowly damped oscillation described by

$$\begin{aligned}F_{m,n}(0,\,t)&\simeq C_{m,n}\frac{\omega_{c,m,n}}{2(1-M^2)^{1/2}a}\left[\frac{2}{\pi(1-M^2)^{1/2}\omega_{c,m,n}t}\right]^{1/2}\\&\quad\times\cos\left[(1-M^2)^{1/2}\omega_{c,m,n}t+\frac{\pi}{4}\right]\end{aligned} \tag{9}$$

where

$$C_{m,n}=\int_{-\infty}^{\infty}F_{m,n}(z,\,0)\,\mathrm{d}z$$

The $t^{-1/2}$ damping law of this oscillation, characteristic of conditions in which oscillation energy is taken away by radiation alone, makes for a long persistence of both cross-mirror and cross-electrode oscillations. As an example, it may be calculated easily that for a mode with $2\pi a/\omega_c = 3$ cm (a typical cross-electrode mode) and an initial amplitude of 0.2 times the initial relative pressure perturbation, i.e., $C_{m,n} = 0.01$ cm corresponding to a discharge width of 3 cm and a relative pressure perturbation of 0.16, the oscillation amplitude reduces to 5×10^{-3} after 2 ms, whereas for $2\pi a/\omega_c = 1$ m (a typical cross-mirror mode) and the same other conditions, it reduces to 1×10^{-3} after 2 ms.

These simple estimates indicate a greater amplitude of cross-electrode modes, which is due to their stronger coupling to the thin discharge, for a comparable level of initial disuniformity; nevertheless, cross-mirror modes do persist for a long time, and in practice may be excited with a large amplitude by the end of the discharge, which is located at a distance from the mirror wall. In addition, it should be noticed that the nozzle leading in and out of the discharge chamber does not maintain a constant cross section, nor do the electrodes themselves, which are curved in order to generate the proper electric field, and these three-dimensional effects affect the short-wavelength, cross-electrode modes much more than the longer-wavelength, cross-mirror modes.

III. Numerical Calculation of Cross-Mirror Waves

After the qualitative analysis of the problem of wave propagation in a uniform-cross-section duct, we shall now undertake a numerical study of cross-mirror waves, with the aim of understanding the local structure of waves caused by the ending of the discharge at a distance from the duct walls where mirrors are located, and of investigating the effect on these waves of varying duct cross section and advection by the steadily moving fluid, both of which were neglected in the preceding analysis.

A preliminary estimate of computational efforts as well as precision requirements in respect of the other approximations present in the model led us to adopt a quasi-two-dimensional numerical model.

Quasi-Two-Dimensional Model

The quasi-two-dimensional formulation of Eq. (2) can be obtained in much the same way as the usual equations of quasi-one-dimensional gas dynamics in a duct. First, the equation of mass conservation $\partial\rho/\partial t + \mathrm{Div}(\rho V) = 0$ is integrated over the cross-electrode y span while taking into account that normal velocity vanishes at the upper and lower walls y^+ and y^-, thus giving

$$\frac{\partial}{\partial t}\int_{y^-}^{y^+} \rho \, dy + \frac{\partial}{\partial x}\int_{y^-}^{y^+} \rho u \, dy + \frac{\partial}{\partial z}\int_{y^-}^{y^+} \rho w \, dy = 0 \qquad (10)$$

Then, the integrals in Eq. (10) are approximated as $h\rho$, $h\rho u$, and $h\rho w$, respectively, h being the height $y^+ - y^-$ and ρ, u, w suitable mean values of these quantities implicitly defined by the approximation itself. The momentum equation is similarly averaged, practically retaining its form unchanged as $\rho \mathrm{D}V/\mathrm{D}t = -\mathrm{grad}\, p$. Substitution into Eq. (10) and linearization with respect to velocity and pressure variations finally give the correspondent of Eq. (2) as

$$\frac{h}{a^2}\frac{\mathrm{D}^2\delta p}{\mathrm{D}t^2} - \mathrm{div}(h\ \mathrm{grad}\ \delta p) = hg \qquad (11)$$

where space derivatives are now calculated with respect to the cross-mirror and streamwise coordinates x and z only, the substantial derivative $\mathrm{D}/\mathrm{D}t = \partial/\partial t + V\partial/\partial z$ is evaluated using the unperturbed steady velocity V (which changes with z as the reciprocal of the duct cross-section size) and h cannot be taken out of the sign of divergence because it is a function of spatial coordinates.

For the purpose of the numerical solution we preliminarily observe that, Eq. (11) being second order with respect to time, it is necessary either to adopt two variables as main unknowns (for instance, pressure and its time derivative) or equivalently to keep track of the values of pressure at two successive time levels. The second choice affords a simpler and faster numerical algorithm (as is also true, in general, for second-order ordinary differential equations[7]) and is therefore preferable. In addition, rather than writing down the derivative $\mathrm{D}^2p/\mathrm{D}t^2$ explicitly in terms of time and space derivatives and discretizing the latter, it is more economical to write the discretized form of Eq. (11) in the reference frame moving with the fluid's velocity, where $\mathrm{D}/\mathrm{D}t$ is the true time derivative, and after each integration step transfer the new values, which are obtained in positions not corresponding to grid sites, back on to the grid by a suitable, separate, convection formula (for instance, third-order interpolation).

Finite Difference Formulation

We start by considering a standard wave equation with no effect of changing cross section and no convection. Assuming equally spaced successive time levels at intervals of Δt and a square grid with spacing Δx, and using the standard three-point finite difference approximation of a second derivative, we may write a simple, second-order-accurate, finite difference discretization of the wave equation as

$$p_{i,j}^{(n+1)} - 2p_{i,j}^{(n)} + p_{i,j}^{(n-1)} = \frac{a^2\Delta t^2}{\Delta x^2}\left[p_{i+1,j}^{(n)} + p_{i-1,j}^{(n)} + p_{i,j+1}^{(n)} + p_{i,j-1}^{(n)} - 4p_{i,j}^{(n)}\right] \qquad (12)$$

where n labels the time levels and i,j identify the mesh point in space. In general, since we are solving a hyperbolic equation that describes waves moving with the speed a, it is necessary, in order to have a time-accurate and numerically stable solution, to choose a time step Δt not exceeding the order of magnitude of $\Delta x/a$ (the precise meaning of this statement depending on the particular numerical method); it is also advisable, in order to contain the running time within reasonable limits, not to choose a much smaller one. In the case of Eq. (12), in particular, there is a special choice consistent with these requirements that offers a definite advantage: setting $\Delta t = \Delta x/\sqrt{2}a$ zeroes the coefficient of $p_{i,j}^{(n)}$ and completely decouples odd from even mesh points. This means that we can get rid of half of the points and obtain the same result, or alternatively reduce the spacing Δx by a factor of $\sqrt{2}$ retaining the same number of points, if only care is taken of the fact that the meshes turn out to be staggered in time. In particular, on rotating the axes used to obtain Eq. (12) by 45 deg, we obtain

$$p_{i,j}^{(n+1)} = -p_{i,j}^{(n-1)} + \tfrac{1}{2}\left[p_{i+\frac{1}{2},j+\frac{1}{2}}^{(n)} + p_{i-\frac{1}{2},j+\frac{1}{2}}^{(n)} + p_{i-\frac{1}{2},j-\frac{1}{2}}^{(n)} + p_{i+\frac{1}{2},j-\frac{1}{2}}^{(n)}\right] \qquad (13)$$

which is an explicit formula to advance the values of pressure in time by $\Delta t = \Delta x/2a$ (Δx being the mesh size along the new i and j directions) starting from two previous time levels, staggered with respect to each other.

We may verify from a different viewpoint that Eq. (13) is a second-order-accurate approximation to the wave equation by taking its Fourier transform with respect to all variables. On doing so, we obtain the dispersion relation

$$\cos \omega\Delta t = \cos \beta_1\Delta x/2 \cos \beta_2\Delta x/2 \qquad (14)$$

which for $\Delta x/2\Delta t = a$ is, as expected, a second-order approximation of the exact dispersion relation $\omega^2 = a^2|\boldsymbol{\beta}|^2 = a^2(\beta_1^2 + \beta_2^2)$ for small β_1 and β_2. In addition, we may observe that ω is always real for real β_1 and β_2, thus giving rise to waves that are neither amplified nor damped, and that Eq. (14) turns out to be exact for waves propagating along the direction of either

axis; in fact, if $\beta_1 = 0$, then ω equals $\pm a\beta_2$ exactly and vice versa. Furthermore, by expanding Eq. (14) in powers of $\beta\Delta x$, it can easily be found that, to fourth order,

$$(\omega\Delta t)^2 \simeq (|\beta|\Delta x/2)^2 - \beta_1^2\beta_2^2\Delta x^4/12 \tag{15}$$

and hence that, for instance, a phase speed error of at most 1% is produced in all directions for $|\beta|\Delta x < 1$.

Corresponding to the quasi-two-dimensional Eq. (11), a simple extension of this procedure leads to the difference equation

$$\begin{aligned} p_{i,j}^{(n+1)} &= -p_{i,j}^{(n-1)} \\ &+ 2[h_{i+\frac{1}{4},j+\frac{1}{4}} p_{i+\frac{1}{2},j+\frac{1}{2}}^{(n)} + h_{i-\frac{1}{4},j+\frac{1}{4}} p_{i-\frac{1}{2},j+\frac{1}{2}}^{(n)} \\ &+ h_{i-\frac{1}{4},j-\frac{1}{4}} p_{i-\frac{1}{2},j-\frac{1}{2}}^{(n)} + h_{i+\frac{1}{4},j-\frac{1}{4}} p_{i+\frac{1}{2},j-\frac{1}{2}}^{(n)}] \\ &/(h_{i+\frac{1}{4},j+\frac{1}{4}} + h_{i-\frac{1}{4},j+\frac{1}{4}} + h_{i-\frac{1}{4},j-\frac{1}{4}} + h_{i+\frac{1}{4},j-\frac{1}{4}}) \end{aligned} \tag{16}$$

where it is assumed that h is known exactly and can be evaluated easily at quarter-step intervals. Equation (16) is second-order accurate and numerically conservative.

Nonreflecting Boundary Conditions

In order to obtain a reasonable numerical representation of wave propagation in just a part of the flowfield (the part of the nozzle around the discharge region) without solving explicitly the equations of motion in the remaining part, it is necessary to provide nonreflecting boundary conditions at the inflow and outflow numerical boundaries where the calculation is terminated. Nonreflecting boundary conditions are basically a replacement for a solution domain extending out to infinity and are derived from the analytical knowledge of the behavior of waves far from their source. There is, however, a distinction between mathematically sufficient boundary conditions (the prototype of which is Sommerfeld's radiation condition), that allow a unique solution to be selected when the position where they are applied tends to infinity, and numerical nonreflecting conditions, that must be able to provide as good as possible an approximation of the infinite-domain solution when applied at a finite and not too expensively large distance. In the present problem, fairly effective nonreflecting conditions are needed because the small step required to resolve the width of the discharge binds us to restrain the calculation domain to an approximately square region where the inflow and outflow numerical boundaries are not really very far from the source.

In a one-dimensional setting, nonreflecting boundary conditions can be provided exactly. In fact, at any point, the solution of the wave equation can be exactly decomposed into a left-going and a right-going wave, and a simple linear equation involving two adjacent points (which is sometimes called an impedance condition) can select one of these waves and bar the generation of the other. For instance, the difference equation

$$p_i^{(n+1)} = -p_i^{(n-1)} + p_{i+\frac{1}{2}}^{(n)} + p_{i-\frac{1}{2}}^{(n)} \tag{17}$$

which is the one-dimensional analog of Eq. (13), represents one-dimensional waves exactly [in fact, its dispersion relation is identical to that of the differential wave equation and its solution can, just as that of the differential wave equation, be expressed as $p = f_+(n - 2i) + f_-(n + 2i)$]; the condition

$$p_N^{(n+1)} = p_{N-\frac{1}{2}}^{(n)} \tag{18}$$

applied at the last point, $i = N$, exactly imposes the absence of left-going waves at that point [because Eq. (18) is exactly verified by the right-going term $f_+(n - 2i)$ only].

In two or more dimensions, matters are considerably different because waves there have a continuum of possible directions. A straightforward generalization of Eq. (18) would appear to be

$$p_{N,j}^{(n+1)} = \tfrac{1}{2}[p_{N-\frac{1}{2},j-\frac{1}{2}}^{(n)} + p_{N-\frac{1}{2},j+\frac{1}{2}}^{(n)}] \tag{19}$$

but, although it can be verified easily by the Fourier-transform method that this condition does not reflect waves traveling parallel to the x axis, in agreement with the one-dimensional result, its partially reflecting oblique waves can be demonstrated both by analytical arguments and by numerical experiments.

In order to provide a better (i.e., practically more useful) numerical nonreflecting boundary condition, we must first specify with greater precision what the nonreflection problem actually is. Our basic aim is, as recalled at the beginning of this section, to obtain a particular (inner) part of an infinite-domain solution without actually approximating the remaining (outer) part numerically. In principle, it is always possible to replace the solution in the outer domain by a functional equation between quantities evaluated on the boundary of the inner domain, a linear integral equation when the starting equations are linear, and in this sense such a functional equation constitutes the perfect nonreflecting boundary condition. However, its practical determination is a slightly more complex problem than the solution of the original equations themselves and may prove possible only for very simple geometries. (In addition, even if it were possible to determine the exact functional equation, as can sometimes be done by a preliminary numerical calculation, or analytically for very special domains, its form would, in general, involve the values of the unknown function over all of the boundary and at all previous times simultaneously, so that its practical application would involve considerable numerical complications.) Notice also that the perfect nonreflecting functional equation depends on all of the properties of the outer solution domain and, in particular, on the shape of its boundary. Therefore, the name of nonreflecting boundary conditions is usually given to imperfect conditions that try to approximate the perfect functional equation by relying on the euristic (that is, not always true) concept that, if no sources exist in the outer domain, waves must cross the boundary in the outward direction only.

In fact, a local distinction between outward and inward waves only makes sense, in more than one dimension, within the context of locally plane waves. Fortunately, it is a characteristic of most wave-propagation problems that waves turn locally plane soon after leaving their sources, so that the problem may be treated one-dimensionally if only the local wave direction is preventively identified. It is relatively easy to transform Eq. (19) into a condition that, in addition to remaining exactly nonreflecting for waves parallel to the x axis, is also nonreflecting for plane waves arriving from any given single direction. To this end, let us give unknown weights w_- and w_+ to the points on the right-hand sides of Eq. (19), rewriting it as

$$p_{N,j}^{(n+1)} = \tfrac{1}{2}[w_- p_{N-\frac{1}{2},j-\frac{1}{2}}^{(n)} + w_+ p_{N-\frac{1}{2},j+\frac{1}{2}}^{(n)}] \tag{20}$$

and let $\hat{d} = (\cos\theta, \sin\theta)$ be a unit vector. A general plane wave traveling in the direction of this unit vector is represented by a function of the form $p = f(at - \hat{d}\cdot r)$. We may impose that this wave is not reflected by choosing the coefficients of Eq. (4) so that Eq. (4) itself is identically satisfied (to leading order in its Taylor-series expansion, at least, as is generally true of difference equations) by this single traveling wave, without the addition of any other term that would represent a reflected wave.

Expanding the function f in a Taylor series to first order as $f \simeq f_0 + f_0'[a(t - t_0) - \cos\theta(x - x_0) - \sin\theta(y - y_0)]$ and inserting the result into Eq. (4) gives

$$\begin{aligned} &[1 - (w_- + w_+)/2] f_0 + [a\Delta t - (w_- + w_+)\cos(\theta)\Delta x/4 \\ &- (w_- - w_+)\sin(\theta)\Delta x/4] f_0' = 0 \end{aligned} \tag{21}$$

Equating the coefficients of f_0 and f_0' separately to zero and remembering that $\Delta t = \Delta x/2a$, gives the two equations

$$w_- + w_+ = 2 \tag{22}$$

$$(\cos\theta + \sin\theta)w_- + (\cos\theta - \sin\theta)w_+ = 2 \tag{23}$$

from which w_- and w_+ may be calculated as functions of θ. The resulting boundary condition (4) will be nonreflecting, to second order, for waves coming along the direction $\hat{d}$; in addition, just as Eq. (3), it will also be exactly nonreflecting for waves parallel to the x axis, as it may be verified that Eq. (23) is satisfied for $\theta = 0$ for any choice of w_- and w_+ consistent with Eq. (22).

We have thus obtained a condition that works for locally plane waves of a given direction. We now make this direction a function of the evolving solution itself, adapting it to the local direction of waves arriving on the boundary. For this purpose, we use the property that, if p has the structure of a locally plane wave, then the gradient of p is directed parallel to the wave vector. We therefore choose the local direction of the discretized gradient as vector $\hat{d}$.

The condition thus constructed has given very good results in the context of the numerical simulations described in the next section, in the sense that no appreciable difference appeared between solutions calculated in domains of different size. The same cannot be said of condition (19), which caused very noticeable alterations to the wave fronts of the transverse waves.

Numerical Results

The algorithm has been applied to the duct geometry depicted in Fig. 2, a 55-cm-long section of a 1.28-m-wide duct in which a rectangular electric discharge with a longitudinal size of 3 cm and a width of 1 m is periodically fired. The particularly elongated shape of the discharge region has made a small mesh spacing unavoidable. Since the configuration is symmetric, only half of the duct has been modeled, by placing 110×128 grid points with a mesh size of 0.5 cm, so that the discharge region encompasses six meshes (the minimum necessary in order that waves of a wavelength equal to the width of the discharge have a phase-speed error lower than 1%). The duct wall is modeled as a perfectly reflecting rigid wall, whereas nonreflecting boundary conditions of the type described in the preceding subsection are imposed at the inlet and outlet numerical boundaries. In all cases, $\gamma = 5/3$ and a speed of sound of 480 m/s (characteristic of neon) have been assumed, together with an energy release of 100 J/l per pulse, an absolute gas pressure of 4 atm (leading to a relative pressure jump of 0.16 and a relative isentropic density jump of $\gamma^{-1}\delta p/p \simeq 0.1$), and a flow speed at the throat of 60 m/s.

Three main effects appeared to be relevant during the numerical simulations.

In a first series of runs the duct was considered as of constant cross section, so as to reproduce the situation considered in the theoretical analysis of Sec. II. When the discharge spanned the whole width of the duct, simple one-dimensional waves, as in Fig. 1, were obtained, which after separation left a relative density defect of 0.1 in the central entropy wave and a relative density increase of 0.05 in each of the two outgoing pressure waves.

When, in a second series, the discharge was let end at a distance from the wall, as in the real device, a cylindrical compression and a cylindrical expansion wave were also emitted from the edge of the discharge in opposite directions. These cylindrical waves bounced back and forth between the lateral walls of the duct and produced the slowly decaying disturbances characteristic of transverse waves.

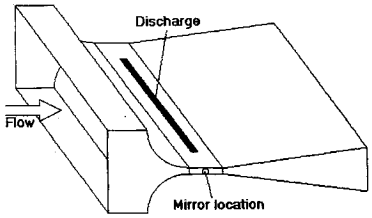

Fig. 2 Nozzle geometry.

The third effect considered was the presence of the convergent-divergent nozzle necessary to drive the gas through the discharge region at a high speed with reasonable aerodynamic efficiency. The nozzle was accounted for quasi-two-dimensionally, in the manner described at the beginning of this section, since its profile extends in the direction orthogonal to the plane of the computation. The main difference observed in the simulations with the nozzle present was that, as the outgoing compression waves entered the upstream and downstream dilations, they began to send back expansion waves, the stronger the more rapid was the dilation, that generated a wide central expansion after about half a millisecond. Interestingly enough, as soon as the upstream wave entered the constant-cross-section region that preceded the convergent part of the nozzle, it sent back a new compression wave that swept away the previous expansion and brought back the pressure and density in the discharge region to their initial values little after 1 ms. It remains to be seen how much this perfect cancellation is real and how much it is due to the quasi-two-dimensional model. Certainly three-dimensionality effects significantly affect the reflection of the main expansion wave from the nozzle because its cross section is not really slowly varying and therefore this reflection, in particular from the convergent section, might in reality be of a different intensity than predicted by the quasi-two-dimensional model.

A fourth effect that was also accounted for, but turned out to be of little relevance, is the presence of a small cavity in the duct wall in correspondence with the location of the mirrors of the optical resonator.

The results of the final simulation with all of these effects simultaneously present may be seen in Fig. 3, where relative density variations in the gas are represented by a gray-scale coding as shown. The wall of the duct, with a small re-entrance in correspondence of the mirror, and the symmetry axis are located 64 cm (128 meshes) apart from each other. An outline marks the 50×3-cm region where the discharge fires. The profile of the nozzle (in a plane orthogonal to the figure) is projected in actual scale as another outline.

Notice that only pressure waves need be, and have been, calculated numerically by finite differences because the position of the entropy wave, which is simply convected with the fluid, can be calculated very easily. This position has been calculated separately and then composed with the finite difference results in order to report the total density variation due to both types of waves in the figures.

At time 0, the discharge fires, causing a sudden increase of pressure with no density change. The situation 100 μs later may be seen in Fig. 3a. The two compression waves (positive density variations) that leave in opposite directions are clearly visible, as is the expansion (density decrease) associated with the entropy wave (the central white vertical band). The whole pattern has moved slightly from the location of the originating discharge (black outline) owing to convection. Expansion and compression half-cylindrical waves originating from the edge of the discharge are also beginning to appear.

The subsequent evolution of the two plane and two cylindrical waves is shown in the following figures. In Fig. 3b, they are clearly seen to grow away from the source. In Fig. 3c (corresponding to 500 μs after the discharge), the upper compression wave has been reflected from the wall and exhibits a slight lag in the central region caused by the mirror cavity. In Fig. 3d (700 μs), the two main plane waves have disappeared out of the computation domain, absorbed by the nonreflecting boundary conditions. The entropy wave, appearing as a vertical low-density (white) band convected with the fluid—indeed, it has been calculated in that way and then superposed on the solution of the wave equation—moves by one discharge length in 500 μs (Fig. 3c) and thereafter no longer interacts with the discharge region.

At the same time, another phenomenon may be observed to happen: as soon as the two main compression waves enter the varying-cross-section parts of the nozzle, they begin to send back expansion waves toward the central region. (The region

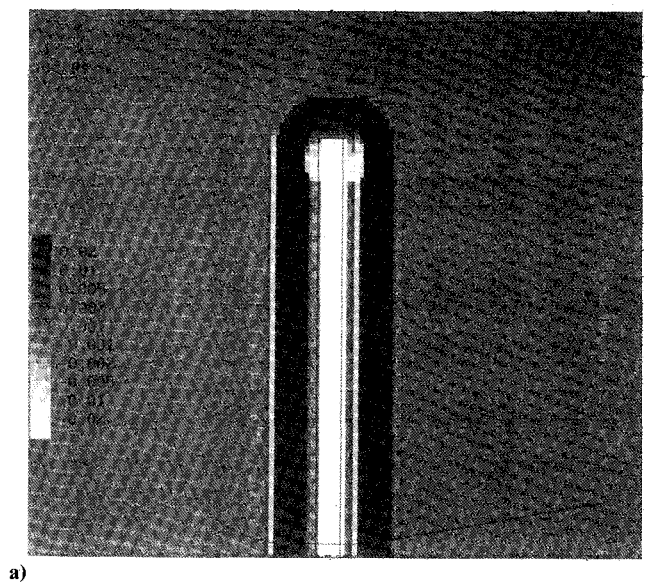

a)

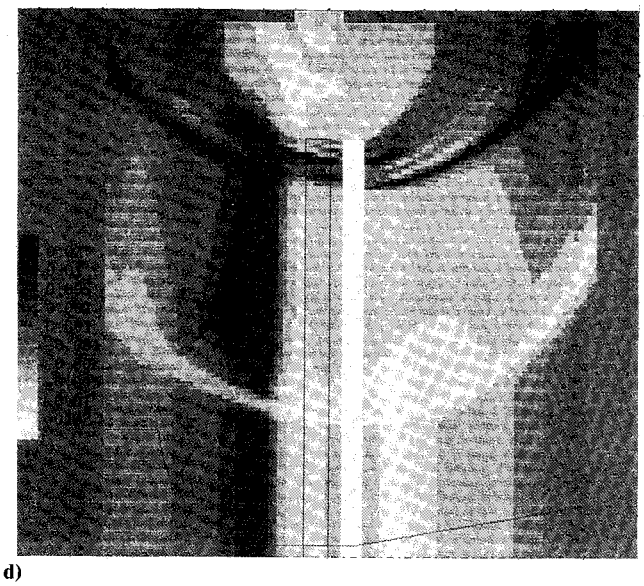

d)

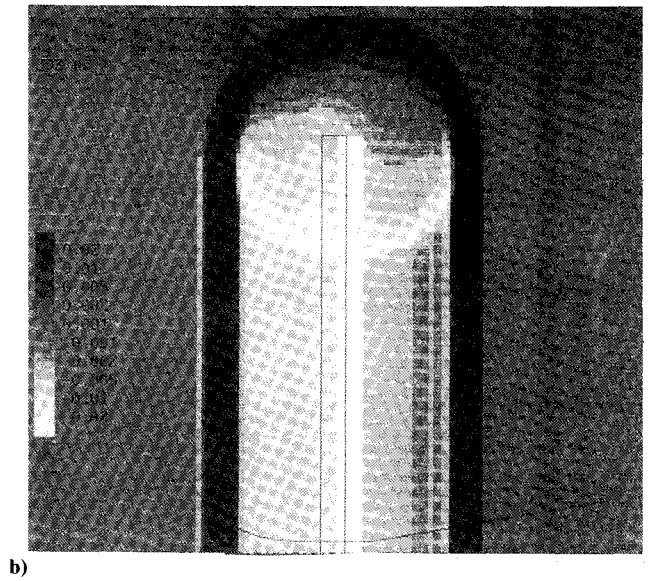

b)

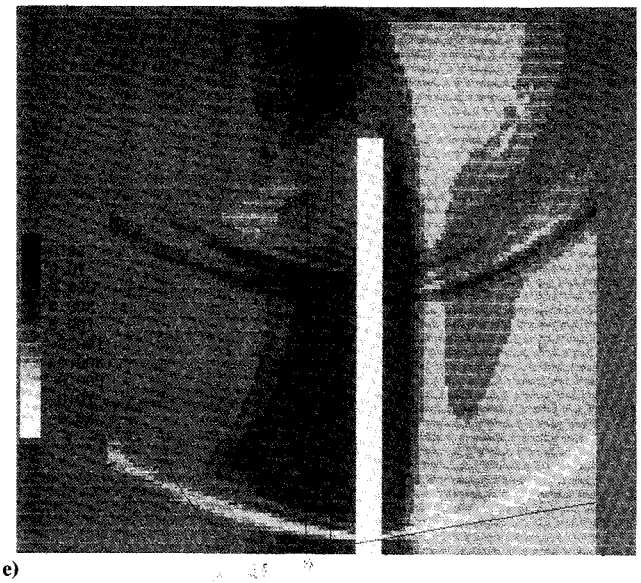

e)

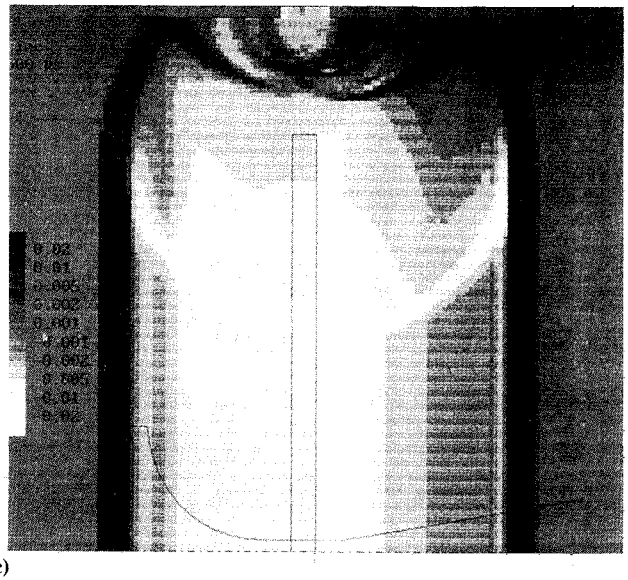

c)

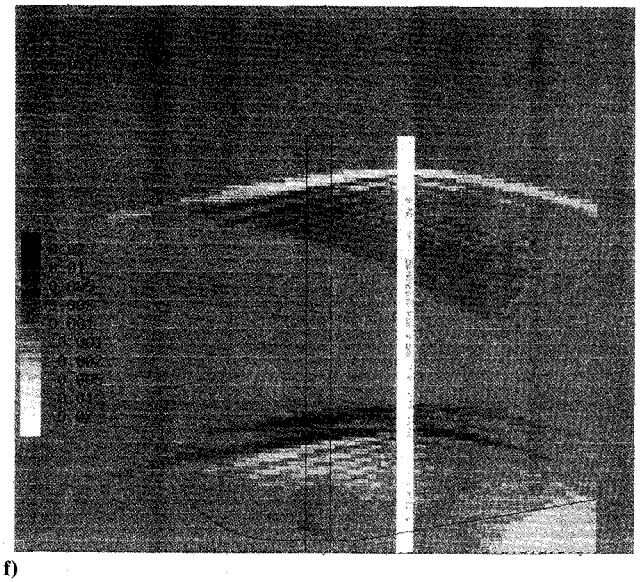

f)

Fig. 3 Density plots (on a gray-level scale) of waves calculated according to the quasi-two-dimensional numerical model at the following times after the discharge: a) 100 μs; b) 300 μs; c) 500 μs; d) 700 μs; e) 1000 μs; f) 2000 μs. The dash-and-dot line at bottom is the symmetry axis. The profile of the nozzle (in a plane orthogonal to the figure) is superposed for reference purposes.

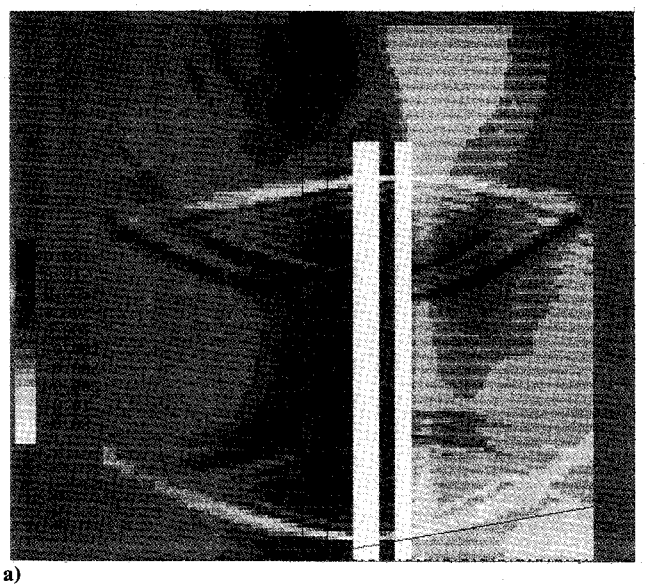

a)

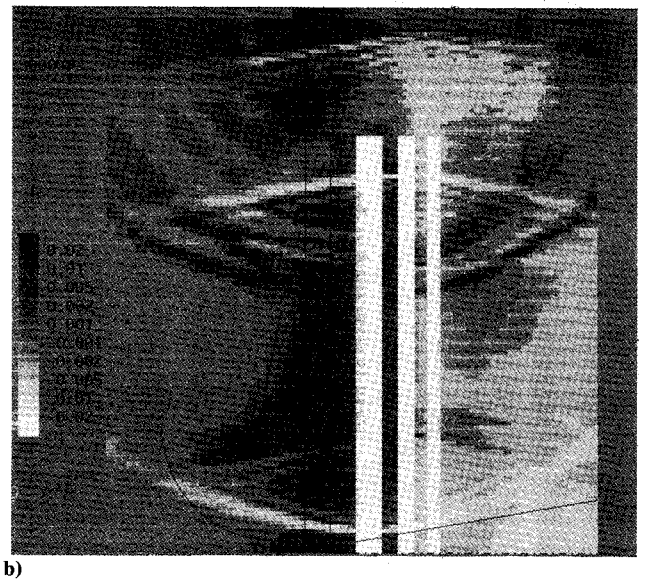

b)

Fig. 4 Density plots of superposed waves produced by two and three successive discharges repeating at 1-ms intervals, at the time of the next discharge: a) two successive discharges, 2000 μs; b) three successive discharges, 3000 μs.

between the waves, which was background gray, i.e., unperturbed, in Fig. 3a, becomes lighter in Fig. 3b, denoting an expansion.) The central expansion becomes stronger and stronger until, in Fig. 3c (500 μs), the left compression wave goes completely past the convergent into the upstream constant-cross-section part; in doing so, it sends back a new compression wave, clearly visible in Fig. 3d, that almost exactly cancels the previous expansion.

Figure 3e shows the situation at 1 ms, when the new discharge would fire for a repetition rate of 1 kHz. As may be seen, both the transverse waves radiated from the edge of the initial discharge and the compression wave reflected from the convergent are still present with nonnegligible intensity in the discharge region (black outline) at this time. Notice that the gray scale has been chosen so that the background shade denotes a relative density perturbation of less than 10^{-3} in modulus. Therefore, any other shade of gray denotes a perturbation higher than 10^{-3}, which is considered potentially dangerous for the stability of the electric discharge.

Figure 3f shows that, as predicted by the theoretical analysis, transverse waves decay very slowly: 2 ms after the discharge the cylindrical waves that radiated from the edge may still be seen going back and forth inside the discharge region with nonnegligible intensity.

Finally, Fig. 4 shows the density field under the superposed effect of several discharges repeating at 1 kHz. The multiple vertical white bands correspond to the low-density, high-temperature entropy waves left behind by each discharge; they become narrower as they move to the right with the fluid because of the cross-section change in the diffuser. The field of perturbations may be seen to be quite complicated, owing to the simultaneous presence of the slowly decaying remnants of many transverse wave fronts.

IV. Conclusions

Analytical estimates and numerical simulations have been performed of the generation of cross-mirror pressure waves by the electric discharge in the EUREKA high-power, high-repetition-rate excimer laser under construction at the national Italian ENEA Frascati laboratories, with particular attention to the attainment of a level of relative density disuniformity lower than 10^{-3}, the estimated threshold beyond which operation of the laser is adversely affected.

Transverse waves propagating along the optical axis are excited, further than by other longitudinal disuniformities of the discharge whose level and typical size ought to be determined experimentally, by the abrupt end of the discharge at a distance from the mirror wall, either when the mirror is located directly on a side of the nozzle or in a suitable lateral pocket. Contrary to cross-electrode waves, these longer-wavelength waves are not expected to be very sensible to the shape of the electrodes, but are significantly affected by the change of the duct cross section in the convergent and divergent parts of the nozzle, and could, in fact, even interact with further structures of the recirculation loop. The effects of cross-section change can be accounted for in a quasi-two-dimensional numerical simulation.

The main result coming out of the simulations is that it is unrealistic to expect a level of density disuniformity of less than 10^{-3} after 1 or even 2 ms from the firing of the discharge with an energy such as to give an equivalent initial density perturbation of 0.1, because of the slow damping (with a $t^{-1/2}$ law, according to the theoretical analysis) of cylindrical transverse waves that, emitted from the edge of the discharge facing the mirrors, bounce back and forth between the lateral walls of the discharge chamber.

The presence of a quasi-two-dimensional nozzle complicates the wave pattern at short times after the discharge, but these effects disappear rapidly because of the perfect cancellation of expansion and compression waves reflected by the nozzle. This conclusion, however, might be modified by three-dimensionality effects.

The presence of a small side pocket in which to locate the mirror, on the other hand, only introduces a slight lag in the central portion of the wave front of the wave reflected by the wall without significant consequences. (However, in other tests performed with a pocket much larger than the one actually foreseen in the device, negative effects did appear because the pocket behaved as a resonator and further enhanced the persistence of transverse waves.)

Optical effects of the waves produced by the discharge were also examined, in respect of both their measurability by interferometric means and their possible negative effects on the quality of the laser beam produced. The refraction-index variations turned out to be too small to produce negative effects on laser beam quality except under extreme spectral-purity requirements. On the other hand, they certainly are big enough to be measured interferometrically. The characteristics of the longitudinal waves reflected by the varying cross section of the nozzle can be experimentally ascertained by such methods, as can those of transverse waves propagating across the electrodes (not studied in the present numerical analysis); however, as long as measurements are taken through the opti-

cal-resonator mirrors, variations associated with waves propagating across the mirrors (i.e., along the line of sight) appear to be too small to be revealed above the background of the longitudinal waves.

Appendix: Nonlinear Interaction of Discharge-Generated Blast Waves

With respect to the linear model in which the pressure field obeys the D'Alembert wave equation while entropy perturbations are transported with the unperturbed stream velocity, two nonlinear effects appear in the complete Euler equations that describe the motion of an inviscid fluid: the convection velocity of both pressure and entropy waves is affected by the perturbation and thus different from the unperturbed fluid speed, and the local speed of sound is affected by changes in the thermodynamic state of the fluid (in particular, by changes of temperature) and thus different from the unperturbed speed of sound. These effects produce an interaction between waves, which in the linear model would simply cross without "seeing" each other; the larger the amplitude of the waves themselves, the stronger is this interaction. Since the greatest perturbation lies in the entropy wave (thermal slug) traveling with the fluid particles that were in the discharge region at the time of the discharge, the largest nonlinear effect that may be foreseen is the partial reflection of pressure waves when they encounter the thermal slug left behind by a previous discharge. In fact, they see the thermal slug as a region where the speed of sound is different, that is, a region of different index of refraction, and a partial reflection is caused by the associated impedance mismatch.

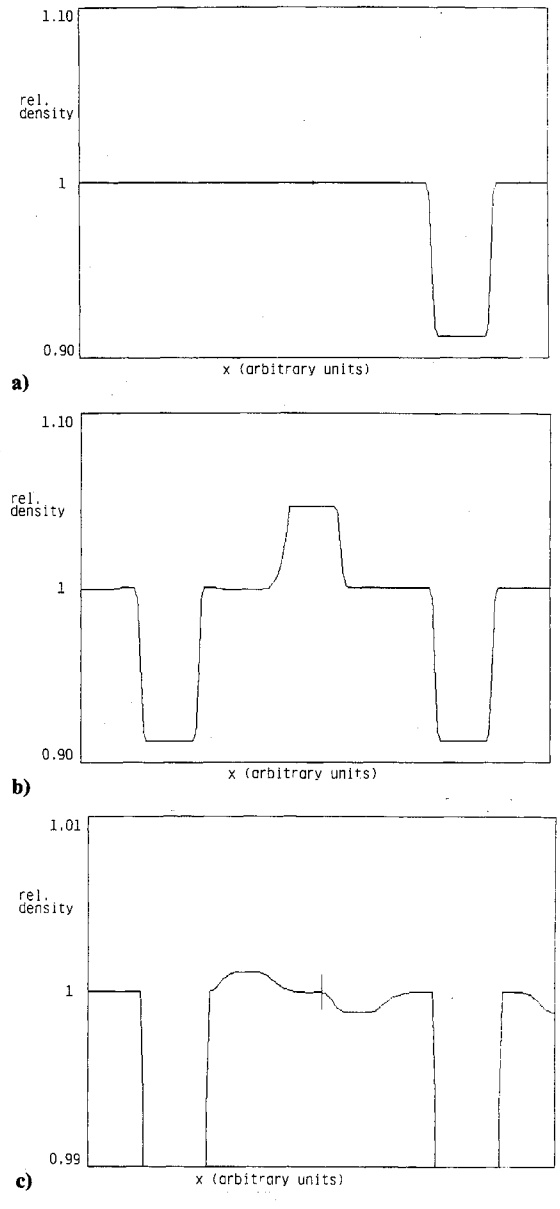

Fig. 5 Nonlinear one-dimensional simulation of pressure-wave reflection upon the entropy wave.

In order to estimate the effects of the nonlinear interaction the pressure waves emitted by any one discharge and the entropy wave of the previous discharge, and in particular the possible partial reflection of the former upon the latter, a wholly nonlinear numerical simulation of their encounter has been performed according to the one-dimensional Euler equations. Figure A1a represents a plot of density vs streamwise coordinate in a frame moving with the fluid and shows (as a density defect) the steady entropy wave left behind by a constant-volume energy increase of 16% of the gas' internal energy (corresponding to an instantaneous energy deposition of 100 J/l in a monoatomic gas at the pressure of 4 atm). At a time when the solution has stabilized in the configuration shown, a second discharge of the same intensity is fired on the left side of the figure. Figure A1b shows, some time later, the two steady entropy (low-density) waves generated by the two discharges together with a pressure wave (density increase at the center of the figure), which is traveling to the right toward the first entropy wave. A left-going pressure wave was simultaneously emitted and has in the meanwhile disappeared out of the calculation domain. The amplitude of the entropy and pressure waves, expressed in terms of relative density variations, is close to the linearly predicted values of -0.1 and $+0.05$, respectively.

Finally, Fig. A1c shows, on an amplified scale, the left-going reflected wave that appears after the pressure wave has gone past the right-side entropy wave. The height of the vertical bar corresponds to a density variation of $\pm 10^{-3}$, and this may be seen to be the approximate amplitude of the reflected wave, roughly 2% the amplitude of the direct wave at the assumed intensity level.

Acknowledgments

This research was funded by ENEA within EUREKA Contract EU213. We are indebted to T. Letardi's work group at the national Italian ENEA Frascati laboratories for bringing this problem to our attention and for providing the necessary details of their ongoing experiment.

References

[1]Cousins, A. K., Thayer, W. J., and Lo, V. C. H., "Long- Wavelength Acoustic Decay in Compact Laser Flow Loops," *AIAA Journal,* Vol. 28, No. 1, 1990, pp. 127–132.

[2]Bessafi, M., Fontaine, B., Forestier, B., Sentis, M., and Zeitoun, D., "Numerical Computation of Unsteady Two-Dimensional Flow in Excimer Laser," *Proceedings of the 7th International Symposium on Gas Flow and Chemical Lasers,* Vol. 1031, 1988, SPIE, Bellingham, WA, pp. 423–427.

[3]Sentis, M., Arif, L., Forestier, B., and Fontaine, B., "Interaction Between Induced Waves and Electric Discharge in a Very High Repetition Rate Excimer Laser," *Proceedings of the 16th International Symposium on Shock Tubes and Waves,* edited by H. Grönig, Aachen, 1987, pp. 911–917.

[4]Baranov, V. Yu., Borisov, V. M., Vinokhodov, A. Yu., Vysikailo, F. I., Gubarev, A. V., Kiryukhin, Yu. B., Krayushkin, I. E., and Laptev, S. A., "Acoustic Vibrations in the Gas-Discharge Chamber of a Fast-Flow Pulse-Periodic Laser," *Soviet Journal of Quantum Electronics,* Vol. 17, No. 6, 1987, pp. 766–770.

[5]Whitham, G. B., *Linear and Nonlinear Waves,* Wiley, New York, 1974.

[6]Morse, P. M., "Linear Acoustic Theory," *Akustik,* edited by S. Flügge, Springer-Verlag, Berlin, 1961, pp. 1–127.

[7]Hamming, R. W., *Numerical Methods for Scientists and Engineers,* Dover, New York, 1973, pp. 414–416.